An Evaluation of Bang-Time Measurements from a Multichannel, Triaxial, nTOF Diagnostic for MagLIF Experiments at the Z facility.

C. L. Ruiz[1a], D.L. Fehl[1b], G. Chandler[1], G. Cooper[2], B. Jones[1], J. D. Styron[2], and J. Torres[1]

[1c]*Sandia National Laboratories, Albuquerque, New Mexico, USA*
[b*]*Retired,Sandia National Laboratories, Albuquerque, New Mexico, USA*
[2]*University of New Mexico, Albuquerque, New Mexico, USA*

1* clruiz@Sandia.gov

ABSTRACT

Neutron bang times for a series of MagLIF (Magnetic Liner Inertial Fusion) experiments [S. A. Slutz, et al., *Phys. Plasma* 17, 056303 (2010)] with D_2-filled targets have been measured at the Z facility [R. B Spielman, C. Deeney, G. A. Chandler, et al., *Phys. Plasmas* 5, 2105]. The emitted neutrons were detected as current-mode pulses in a multichannel, neutron time-of-flight (nTOF) diagnostic with conventional, scintillator-photomultiplier-tube (PMT) detectors. In these experiments, the detectors were fielded at known, fixed distances L (690—2510 cm) from the target, and on three, non-coplanar (but convergent) lines-of-sight (LOS). The *primary goal* of this diagnostic was to estimate a fiducial time (bang time) relative to an externally generated time-base for synchronizing all the diagnostics in an experiment. *Recorded* arrival times (AT) of the pulses were characterized experimentally by three numerical methods: a first-moment estimate (centroid) and two nodal measures – Savitzky-Golay (SG) smoothing and a single-point peak estimate of the raw data.. These times were corrected for internal detector time delays (transit and impulse-response-function) – an adjustment that linked the *recorded ATs* to the corresponding arrival of *uncollided neutrons* at each detector. The bang time was then estimated by linearly regressing the arrival times against the associated distances to the source; t_{bang} (on the system timescale) was taken as the temporal intercept of the regression equation at distance $L = 0$. This article reports the analysis for a representative shot #2584 for which (a) the recorded *ATs* – even without detector corrections – agreed by method in each channel to within 1—2 ns; (b) internal corrections were each ~3 – 5 ns; and (c) a 95% uncertainty (confidence) interval for t_{bang} in this shot was estimated at ±3 ns with 4 degrees of freedom.

A *secondary goal* for this diagnostic was to check that the bang time measurements corresponded to neutrons emitted by the D(d,n)^{3}He reaction in a thermalized DD plasma. According to the theoretical studies by Brysk [H. Brysk *Plasma Phys*, 15 611 (1973)], such neutrons should be *emitted* with an isotropic Gaussian distribution of mean kinetic energy $\overline{E}$ of 2.449 MeV; this energy translates to a mean neutron speed $\overline{u}$ of 2.160 cm/ns [D. H. Munro, *Nuclear Fusion*, 56(3) 036001 (2016)]. In the MagLIF series of shots there was no evidence of spatial asymmetry in the time-distance regressions, and it was possible to extract the mean neutron speed from the slope of these fits. In shot 2584 $\overline{u}$ was estimated at 2.152 cm/ns ± 0.010 cm/ns [95 % confidence, 4 dof] and the mean kinetic energy $\overline{E}$ (with relativistic corrections) was 2.431 MeV ± 0.022 MeV [95 % confidence, 4 dof] – results supporting the assumption that D-D neutrons were, in fact, measured.

*Sandia National Laboratories is a multi-mission laboratory managed and operated by National Technology and Engineering Solutions of Sandia, LLC., a wholly owned subsidiary of Honeywell International, Inc., for the U.S. Department of Energy's National Nuclear Security Administration under contract DE-NA-0003525. The views expressed in the article do not necessarily represent the views of the U.S. Department of Energy or the United States Government.

I. Introduction

From its beginnings in molecular-beam experiments [1], the time-of-flight technique (TOF) has become a mainstay for studying the dynamics of energy-distributed particle beams in physics and chemistry. Conceptually, TOF is simple: in the absence of external fields and material interactions, the speed u of a particle may be estimated by measuring its time-in-flight (TIF) over a known distance L. The TOF strategy has been used for weak beams in particle-counting mode [2,3] and for intense beams in current mode. In particular, the technique (nTOF) has been applied to neutron-emitting, high-density-high-temperature (HDHT) plasmas in inertial-confinement fusion (ICF) experiments [4—10]. The time-dependent spectra of *uncollided* neutrons from an ICF target can be related to (a) a time t_{bang} as fusion neutrons are produced; (b) the neutron yield; (c) an effective ion temperature; and (d) a neutron spectrum $\partial N/\partial E$ – fine details of which probe the interior conditions within the burning plasma.

In its MagLIF (Magnetic Liner Inertial Fusion) [11—13] approach to inertial confinement fusion (ICF), Sandia National Laboratories (Albuquerque, New Mexico) has fielded a multichannel, nTOF diagnostic for D_2-filled targets at the Z facility[14,15]. The primary purpose of this diagnostic is to establish a t_{bang} for neutron production in these experiments on an external, system-provided 'clock', against which other diagnostics can be synchronized. A secondary goal is to determine if the neutrons produced are consistent with the D(d,n)^{3}He reaction from a Maxwellian plasma by estimating the

average speed $\bar{u}$ and symmetry of neutrons in the *uncollided* flux.

The diagnostic configuration adopted here with standard scintillator-photomultiplier detectors (PMT) [16,17] was novel for several reasons: (a) to avoid complete saturation of the scintillators by intense bremsstrahlung and other x-ray backgrounds from the Z accelerator, the detectors could be fielded no closer than ~ 7 m from the neutron source, nor farther than ~25 m to avoid signal interference from backscattered neutrons; (b) widely-spaced, multiple detectors enhanced the resolution of neutron $t_{\mathbf{bang}}$ and $\bar{u}$ estimates; and (c) the detectors were distributed over three independent lines-of-sight (LOS) to permit coarse checks for spatial asymmetries in neutron emission. Of course, the price paid for moving the detectors away from the source was spatial and temporal spreading of the emitted neutron burst as well as increased exposure to backscattered x rays and neutrons from the massive, support structures in the Z accelerator. Such interferences made fine details of the neutron spectrum beyond the scope of the these studies. Thus, compared to neutron times-in-flight, the plasma lifetime was essentially instantaneous.

Because the time-dependent, nTOF data $D_k(t)$ in each k detector comprises a single (often noisy and deformed) pulse, the major challenge for analyzing the MagLIF data was in identifying some temporal feature(s) in the *recorded* signal that can be directly traced to uncollided neutrons incident on each scintillator *and* then further back to the source plasma itself. This cannot be done with imprecise notions of 'peak time' in the recorded traces. Rather, in the presence of noise, interference, and signal distortion, it is imperative to define and to test consistent procedure(s) for estimating data 'arrival times' (AT) at the nTOF detectors and then neutron 'time-in-flight' (TIF) as a function of the distance to the source L. Then $t_{\mathbf{bang}}$ can be defined as the limit of this function as $L \to 0$.

Reported here are estimated 95% confidence intervals for $t_{\mathbf{bang}}$ in MagLIF shot #2584, a representative experiment with a D_2-filled target. Also reported is the mean neutron speed $\bar{u}$ (with uncertainties) in this shot and the mean neutron kinetic energy $\bar{E}$, both of which agreed with published values for the D(d,n)^{3}He reaction and predictions from Maxwellian plasma models [4,5].

This article is comprises five major sections. An nTOF measurement at Z is basically a set of k = 1,.., M = 6, neutron detectors, arranged at varying distances L_k from a plasma source. Sect. II summarizes the basic geometry for these experiments; compares traces of raw and smoothed *recorded* data $D_k(t)$ with comments on signal reproducibility and perturbations; and suggests simple measures for establishing arrival times. The purpose of Sect. III is then to demonstrate that such operational definitions can be justified within the context of a typical nTOF experiment. Three methods are considered: specifically, $(t_{\mathbf{smoo}}, t_{\mathbf{mode}})$ variants of 'peak-signal' estimates and $\langle t \rangle$, a 'mean-time' estimate over a restricted (FWHM) time-domain (centroid). A mathematical model is posited for linking such arrival times to $t_{\mathbf{bang}}$ and $\bar{u}$. Section IV displays the results for these methods on raw data in shot #2584, fits the linear model of Sect. III to these data, and extrapolates to $t_{\mathbf{bang}}$ on the system timescale; this section also shows the effects of detector response times, leading to a corrected $t_{\mathbf{bang}}$. Lastly, Sect. V describes how 'back-of-the-envelope' calculations corroborate these measurements, compares the measured speed $\bar{u}$ and inferred $\bar{E}$ here to published values, and speculates about future work.

II. Experimental Configuration and Raw Data #2584

A. Geometry

Figure 1 shows a perspective view of the Z accelerator at the Z facility. Overall, the accelerator is cylindrically symmetric about a vertical polar axis passing through a concentric, vacuum target chamber (3.66 m in diameter and 7.62 m high); a MagLIF target is placed at the center of this chamber. Marx generators, storage capacitors, pulse-forming lines, switches, and a plastic insulation stack (immersed in either oil or water) surround the target chamber. Outside the target chamber, various radial lines-of-sight (LOS) diverge in a spherical-polar coordinate system centered on the target and polar axis (with the z-axis pointing downwards, so that points above the accelerator have azimuth angles greater than 90°.)

For multichannel nTOF studies, seven nearly-matched, scintillator-PMT detectors were mounted to three, non-coplanar LOSs at varying distances from the target to measure neutron arrival times and to check for anisotropy in neutron emission. Each detector string (scintillator-light-guide-PMT) was independently calibrated for sensitivity and temporal response vs. PMT bias voltage [16]. Some detectors were in fact 'dual' (BA2, BA3) in that two PMTs viewed the same scintillator in opposed directions. The channel names and their locations L_k are listed in Table I. (One channel of a dual detector was completely lost due to noise and is not included here.). The radial source-to–scintillator distances (SSD) L were measured with a graduated, steel tape which was (just) able to distinguish length increments down to ~ 0.07 cm (1/32 inches); but, the overall accuracy of L was estimated to be ±1 cm, due to sagging of the tape, shock motion and thermal expansion of both the LOS and the tape. Taking such systematic error estimates as $\delta L \sim 0.5 - 1$ cm still yields fractional estimates $\delta L / L \sim 0.1$ % over the various LOSs (Tbl. 1); and for 2.4-MeV DD-neutrons, such length-errors represent arrival-time errors of ~0.25–0.5 ns. (Nevertheless, in Tbl. 1 length precisions of 0.01 cm have been retained to reduce unnecessary round-off-errors in the subsequent statistical analysis.)

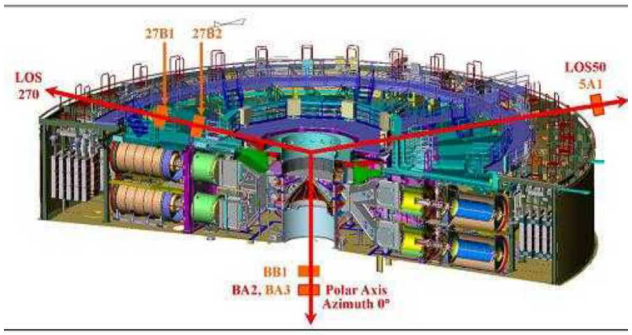

Figure 1. (Color Online) Perspective view of the Z accelerator for MagLIF target experiments and of the lines-of-sight used for nTOF measurements (not to scale). Depicted inwards from the oil-tank wall are Marx generators, storage capacitors, pulse-forming lines and the insulator stack; not shown is the MagLIF target chamber itself. Labeled NTOF detector locations are shown on the various diverging lines-of-sight and correspond to Table 1.

Distance (cm) L,k	Channel Name	Polar (deg.)	Azimuth (deg.)
689.64	BB1	n/a	0
785.98	BA2	n/a	0
785.98	BA3	n/a	0
944.56	27B2	270	110
1145.85	27B1	270	110
2510.00	5A1	50	110

Table 1. SSD L_k (cm), polar and azimuthal angles of detectors for MagLIF for DD-neutron TOF study, shot #2584. The co-ordinate system is spherical-polar with the polar axis pointed downwards, so that detectors at 690 and 786 cm are below the target while the others are above the target. The detector at 2510 meters is on a third axis..

B. Data from a Representative MagLIF Shot

Figures 2–5 show time-series data $D_k(t)$ from shot #2584 for the six useable channels and are keyed to Tbl. 1. These traces were recorded by 8-bit, 1 GHz digitizers with 0.25 ns dwell times. All represent what we call here 'raw data' in the following sense: (a) baselines were locally corrected; and (b) temporal corrections were made for *nominal* PMT throughput times. What is *not* corrected in these raw data are temporal adjustments due to individually calibrated [16] detector impulse-response functions (IRF) and to actual throughput times; such adjustments vary slightly from one detector-string to another and depend on the PMT-bias voltage settings. The corrections are typically, however, are □5 ns in magnitude for a given channel and altogether shift t_{bang} by a few ns in the final analysis. (Cf. Sects. III.B and IV.B.) The traces in Figs. 4 and 5 have been additionally smoothed with the Savitzky-Golay technique [18,19] (See Sect. III.) to simplify comparisons here.

Taken in order, these figures show the following:

Fig. 2 shows the BB1 channel (the detector closest to the source) on a 700 ns timescale. The off-scale pulse at 3000 ns (on the system clock) corresponds to bremsstrahlung from the voltage divider stack attached to the target holder pulse plus target x rays; the neutron pulse is the tiny peak at ~3430 ns. (The time-in-flight of a 2.45 M D-D neutron to this detector is also indicated.) The point is that since the nTOF detectors used at Z cannot discriminate between neutrons and hard x rays, moving them significantly closer to the source for t_{bang} time measurements invites more troublesome x-ray backgrounds.

Fig. 3 compares the variation of noise-to-signal among the raw neutron signals. Shown here are channel BB1 (lower trace, at 689 cm from Fig. 2 on a narrower timescale) and channel 27B2 (upper trace, at 945 cm) which peaks ~100 ns later than BB1. (27B2 has been arbitrarily shifted and scaled.) On this scale neither trace shows the full perturbing x-ray pulse in Fig. 2. The noticeable difference in noise-to-signal in these traces comes from the signal range in the two digitizations: without a prominent x-ray background, 27B2 could be adjusted for near full-scale digitization, whereas the BB1 neutron signal could not be. Most of the noise seen in BB1 is quantization noise.

Figure 4 addresses reproducibility. Channels BA2 and BA3 were constructed in one detector housing with two matched PMTs looking at the same scintillator. The traces shown have been smoothed, aligned in time at peak (shift ~1.3 ns), and scaled. One notices individual PMT characteristics ~6 ns after peak and then further agreement. Similar agreement in features is also obtained 20 ns before and 15 ns after peak.

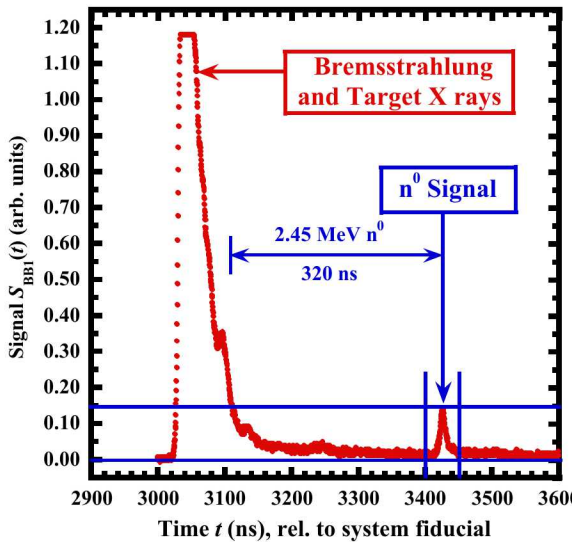

Figure 2. (Color Online) Raw data from shot #2584 for channel BB1 with an early, off-scale bremsstrahlung signal and extended tail, together with a small DD fusion neutron signal (2.45 MeV, peak speed 2.164 cm/ns).

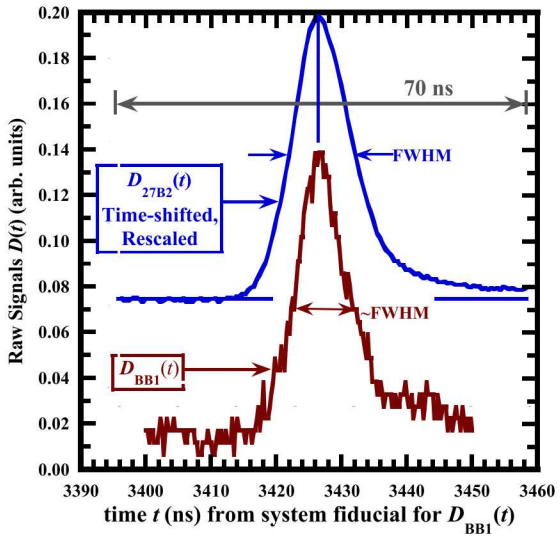

Figure 3 (Color Online) Overlay comparison of noise to signal in raw data vs. time between the worst and 'best' nTOF channels, respectively, BB1 and 27B2. (Data from channel 27B2 has been shifted earlier by 118 ns and rescaled in this comparison.)

Figure 5 shows a composite of all 6 raw data traces obtained in shot #2584. (These have been smoothed, and aligned at peak.) It is clear from these figures that all of the nTOF show mono-modal pulses that are skewed somewhat positive (i.e., displaying a higher falling tail) at late times. As one would expect, the FWHMs increase with distance from the source. The shapes of the pulses are most similar for times within their respective FWHM. The notable exception is channel 5A1 at 2510 cm from the source, which has less shielding than the rest of the detectors – its signal is given particular scrutiny in Sect. V. The Brysk theory [4,5] expects that the *uncollided* neutron pulse should be Gaussian in shape (See Sect. III.A), and it may indeed be so. But, if so, then further analysis of how the *recorded* pulses response to incoming neutrons (either uncollided or not) must be included in determining corrected neutron arrival times data.

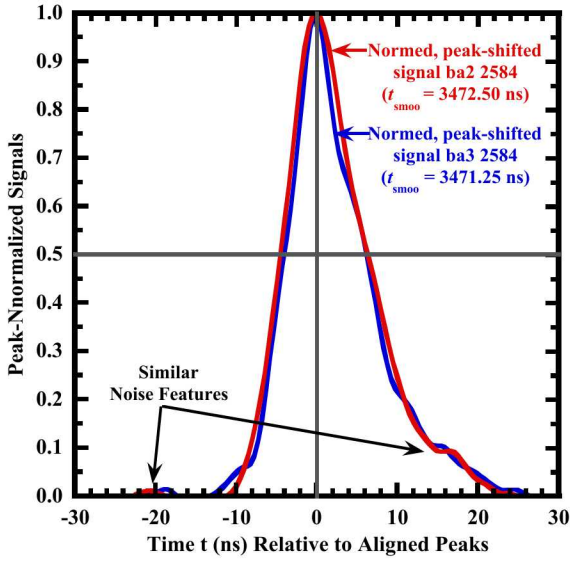

Figure 4. (Color Online) Overlay comparison of (smoothed) signals from the dual, two-channel detector (BA2 and BA3) In this case, the recorded signals were closely similar in shape and separated by 1.3 ns..

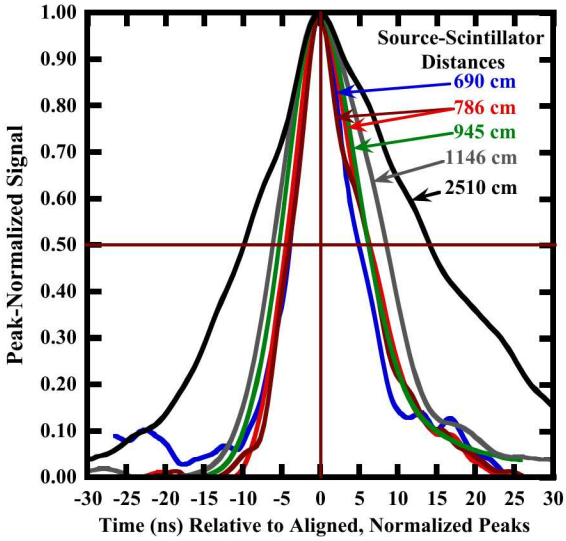

Figure 5. (Color Online) Comparison of all 6 useful nTOF channels in shot #2584, smoothed, normalized and aligned at peak (t_{smoo}). The FWHM is noted. Signals above the FWHM are roughly symmetric, with the exception of signal 5A1, located at 2510 cm from the source.

III. Methods of Data Analysis

The goal of this section is to illustrate what is *not so simple* about nTOF experiments, at least at Z. Overall, the question is this: how does an instantaneous burst of D-D neutrons translate into multiple, *recorded* digital signals; and what can be experimentally inferred about bang time and average speed of the emitted neutron distribution? There are, in fact, several issues that need to be addressed here before one can even estimate just the bang time: (a) What temporal neutron distribution would one predict for a Maxwellian deuterium plasma at an effective temperature from the Brysk model [4]? (b) How may interference signals and noise be reduced within the Z environment? (c) How do instrumental response and throughput times relate the incoming neutron pulses on

the scintillators to the recorded data pulses? and (4) How characteristic feature(s) in the recorded pulse can be consistently defined for the arrival time(s) of neutrons? These questions are pursued in this section.

A. The nTOF Model According to Brysk

The traceability of recorded neutron arrival times to consistent estimates of bang time and average neutron speed $\bar{u}$ depends firstly on conditions within the source plasma and the propagation of neutrons between the source and the scintillators.

According to Brysk [4], *if* a D–D plasma has a Maxwellian distribution, the emergent neutrons at bang time should have a differential energy spectrum $\partial N/\partial E$ of the form:

$$\left(\frac{\partial N}{\partial E}\right) = A \exp\left[-\frac{(E-\bar{E})^2}{\sigma_T^2}\right], \qquad (1)$$

where $\bar{E}, \sigma_T$, and E have units of energy; and the constant A has units of neutron density per unit energy. This is, of course, a Gaussian distribution, where $\bar{E}$ is both the the average neutron kinetic energy (2.45 Mev) for the D(d,n)^{3}He-reaction as well as the mode of $\partial N/\partial E$; σ_T represents the energy spread and depends on the (effective) plasma temperature T.

For the sake of consistent terminology, we shall call neutrons that encounter no material interactions in transit to the nTOF detectors as part of *uncollided neutron flux* at a point in space and time and retain the kinetic energy and momenta with which they were born. According to the Brysk model, this flux provides traceability to the underlying conditions in the plasma. Any other neutrons or x rays interacting with the nTOF detectors then represent signal interferences.

An nTOF diagnostic is a useful spectrometer for such uncollided neutron measurements, over a fixed but known distance L because it experimentally transforms the uncollided distribution $\partial N/\partial E$ into a temporal distribution at each distance L_k. That is,

$$\left(\frac{\partial N}{\partial t}\right)\Big|_k = \left(\frac{\partial N}{\partial E}\right)\left(\frac{\partial E}{\partial t}\right) \cong -A\left(\frac{2\bar{E}}{\bar{t}_k}\right)\left(\frac{\bar{t}_k}{t}\right)^3 \times \exp\left[-\frac{\bar{u}^2\bar{E}^2}{\sigma_T^2 L_k^2}(t-\bar{t}_k)^2\right]. \qquad (2)$$

Here, t is the *time-in-flight of an uncollided neutron from its birth at the plasma* (with kinetic energy E); the *non-relativistic* parameters $\bar{E}$, $\bar{u} \equiv \sqrt{2\bar{E}/m_0}$, and $\bar{t}_k \equiv L_k/\bar{u}$ are the mean kinetic energy, speed, rest mass, and time-in-flight (TIF) of 2.45 MeV neutrons between the plasma and the k^{th} scintillator. Equation (2) is approximately Gaussian (with variable amplitude and width) if the uncollided neutrons are emitted simultaneously compared to clock time and if $|t-\bar{t}_k|/\bar{t}_k \ll 1$ [(e.g., for BB1 ~ 5-ns (FWHM)/320-ns (flight-time) ≈ 1.5%]. Thus, while Eq. (2) does not exactly represent a simple Gaussian shape for uncollided neutrons, *for convenience* we will still refer to it as gaussian distribution $G(t)$ in time, especially at signal points within its half-width.

Experimentally, one does not directly measure the TIF in Eq. (2), but rather arrival-times relative to the recording system fiducial. On the system clock the arrival of an uncollided 2.45 MeV arrives at t_{bang} plus the time-in-flight to the k^{th} scintillator plus a correction for the detector:

$$\underbrace{\bar{t}_k}_{\text{clock time}} = \underbrace{t_{\text{bang}}}_{\text{clock time}} + \underbrace{(\bar{u})^{-1}L_k}_{\text{TIF}} + \underbrace{\delta t_k}_{\text{detector}} \quad . \qquad (3)$$

Once experimental estimates of arrival times are determined, then Eq.(3) can be used in a linear Least-Squares (LS) regression model from which to estimate the bang time on the system clock..

B. Coping with Interference Backgrounds and Noise in MagLIF experiments at Z

As noted above for Figs. 2—5, the raw data traces in shot #2584 are not analytically smooth functions but rather hint at competing physical effects — here *interferences* — which include prompt and scattered x rays from the pulsed-forming lines as well as late-time backscattered neutrons. In addition, there can be noise on cables due to direct x-ray/neutron interactions and quantization 'noise' in the recording system. All these effects are expected in the MagLIF setting and are site specific. Lerche[6], Hatarik [7], and Murphy [8—10] have delineated such issues for the NOVA and NIF installations as well as some mitigating schemes. (For example, (Stoeckl [20] has also reported a gated liquid scintillator.)

As largely experimental problems, such interferences – once identified – may require mitigation by purely empirical means and statistical simulations. For example, as mentioned above, early time x-ray interference in close-in nTOF channels (BB1) was successfully reduced by moving the detectors farther way from the source. Similarly, backscattered neutrons which arrive after the uncollided flux could frequently be ignored by analyzing the raw time signal only within the recorded FWHM domain. Alternatively, one can try to simulate scattered background signals using the Monte Carlo technique [6,7] and then to identify significant scattering sources: this method proved to be somewhat problematic at Z, given the massive number of complicated accelerator structures near the nTOF detectors and the custom shielding and collimation required. Lastly, it was found that the primary random noise in the raw nTOF signals was quantization noise in the digitizers and could be reduced to acceptable levels with Savitizky-Golay smoothing [18,19] and simple averaging techniques. (See Sect. III.D below.)

C. Detector Distortions

The final connection of the recorded data $D_k(t)$ to uncollided neutrons in the k^{th} nTOF detector is its particular response to neutrons in the scintillator → light-pipe → PMT → electrical current processes. Each of these sub-stages requires time to complete, but the net temporal result can often be summarized by an impulse response function (IRF), $R_k(t)$, and a throughput time of the assembled detector. While in some formulations the IRF includes the transit time through the PMT, we have chosen to deal with these separately. The impulse response functions for complete nTOF detector strings as used above at Z have been studied with pulsed x rays and cosmic rays and fit to exponentially-modified-gaussian functions (EMG) by Bonura [16]. (Such four-parameter functions are particularly applicable for data pulses.[21—23]. Bonura found pulse widths of ~3–4 ns (fwhm), and throughput times of 11–13 ns were obtained; these values slightly varied with the specific PMT used and depended on the bias voltage.

One can show [24] that *if* the detection processes for nTOF detectors are all linear, continuous, and superposable (e.g., unsaturated and independent of each other), then the electrical output $D_k(t)$ from the detector can be written as

$$D_k(t) = \underbrace{\int_{-\infty}^{\infty} R_k(t')G_k(t-t')dt'}_{R_k * G_k} + \varepsilon_k(t), \qquad (4)$$

where $R_k(t)$ is the response function (either parameterized or empirically determined) and $G_k(t)$ is a temporal function at position k that one wishes to know something about. This integral is the formal convolution, $R_k * G_k = G_k * R_k$, of $R_k(t)$ and $G_k(t)$. The additional term $\varepsilon_k(t)$ represents non-differentiable noise. In time-series problems measurements, $R_k(t)$ is typically constrained: $R_k(t \geq 0) \geq 0$ (but 0 for $t < 0$).

With response function and recorded data in hand, one is tempted to attack Eq. (4) directly as an unfold problem to obtain $G_k(t)$ point by point. This quest is frequently troublesome because of the noise term $\varepsilon_k(t)$ and a lack of physically realistic, *a-priori* constraints. The issues for this problem have been extensively discussed in the literature, [25—28].

The analysis of NIF nTOF data has been reported Hatarik, et al. [6—10]. Their approach is to give up on direct pointwise reconstruction of $G_k(t)$ and to represent it by an *a-priori*, constraining function based on the Brysk model for which the convolution in Eq. (4) can be performed. The resulting function – the ***EMG***(t) function [22,23] – can then be used as a fitting function and the resulting parameters related to functional moments of $G_k(t)$.

This method was not used for the MagLIF nTOF experiments here because estimating bang time does not require such detailed analysis and the data is of poorer quality than at NIF. One is only looking for temporal feature(s) or averages in $D_k(t)$ that reliably map into similar features in $G_k(t)$. If one is willing to assume that both $R_k(t)$ and $G_k(t)$ are known at least in form (either by measurement [16] and from the Brysk theory, respectively), then some properties of Eq. (4) with respect to Gaussian functions of time apply: specifically, one can show that (a) the mode and the centroid coincide for Gaussians; (b) the mode of the convolution $R_k * G_k$ is the sum of the individual modes of $R_k(t)$ and $G_k(t)$ [29,30]; and (c) the individual centroids also sum in $R_k * G_k$ [30]. [To preserve causality, it has also been assumed here that the approximated response function $R_k(t)$ is essentially zero-valued a FWHM earlier than its mode.]

Hence, in principle, one can estimate the arrival of the *uncollided* neutrons by subtracting off the FWHM of the IRF (approximately) from the corresponding time in the recorded data. This correction then makes a direct connection to the recorded data to the plasma and ultimately to the bang time on the system clock – given the proper inclusion of the PMT throughput time.

D. Operational Methods for Estimating Recorded Signal Arrival Times at Z.

Given now an approximate theoretical connection between the recorded data $D_k(t)$ and the hypothesized uncollided neutron pulse $G_k(t)$, we define recorded pulse arrival times in terms of mode and mean (centroid) properties of the $D_k(t)$, knowing that eventually corrections are needed for detector response and throughput. Three numerical estimates in each channel were labeled as follows: (a) $t_{\mathbf{smoo}}$, (b) $t_{\mathbf{mode}}$, and (c) $\langle t \rangle$, where the names suggest the numerical methods used. The values obtained are compared in Table 2 (Sect. IV), and have *not* been corrected as noted but are studied below. Such corrections are of the order of a few nanoseconds.

The Savitzke-Golay (SG) method is a low-pass digital filter for equally-spaced time-domain data that has been well-described in the literature [18,19]. It transforms a discrete, noisy signal, like $D_k(t)$, into a smoothed signal $D_k^{\mathbf{smoo}}(t)$ based on local polynomial averages. Both the polynomial degree and the width of the averaging window can be selected.

Figure 6 shows the results of applying the SG method to the trace $D_{\mathbf{BB1}}(t)$ in Fig. 3. The filter comprised 4th degree polynomial with a 21-point smoothing window over the 201 points between 3400 ns ≤ t ≤ 3450 ns. Both

the raw data and smoothed result $D_{BB1}^{smoo}(t)$ are shown for comparison. To aid this appraisal, the overall domain in Fig. 6 has been divided into three nesting sub-domains of interest: (a) [3400, 3450] ns, which includes extended baseline noise; (b) [3416, 3436] ns, which approximately excludes this noise; and (c) [3422, 3431] ns, which excludes points outside the FWHM region. The agreement between $D_{BB1}(t)$ and $D_{BB1}^{smoo}(t)$ is very close in each of these regions, with scant evidence on this scale of systematic distortion in $D_{BB1}^{smoo}(t)$. (Although not discussed here, the residuals between the raw and smoothed data are normally distributed about the smoothed curve with a mean displacement of ~2×10^{-6} vertical units and a standard deviation of 0.0039, consistent with the digitization increment in the raw trace of 0.005 units, which the SG process averages over.)

But, the real utility here of the SG method is that both $D_{BB1}^{smoo}(t)$ and its derivative are smooth, so that the smoothed-signal mode, t_{smoo}, can be defined where $\partial D_{BB1}^{smoo} / \partial t$ crosses 0. This determination is shown in Fig. 7 where t_{smoo} = 3426.50 ns (relative to the system time fiducial). Also, noted are the derivative values for the four nearest temporal neighbors (A—D) of t_{smoo}, spaced at 0.25 ns; together these points span a 1-ns time interval and suggest an uncertainty of □ 1 ns for estimating t_{smoo} by this method.

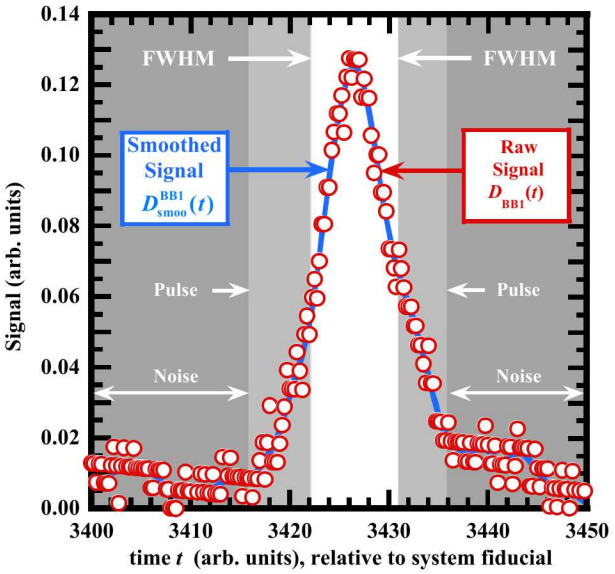

Figure 6. (Color Online) Comparison of the data pulse for channel bb1 vs. the signal smoothed by the Savitzky-Golay digital filter. The peak parameter t_{smoo} is thus calculated from the entire raw signal. Arbitrarily defined sub-domains (noise, pulse, and FWHM) are indicated.

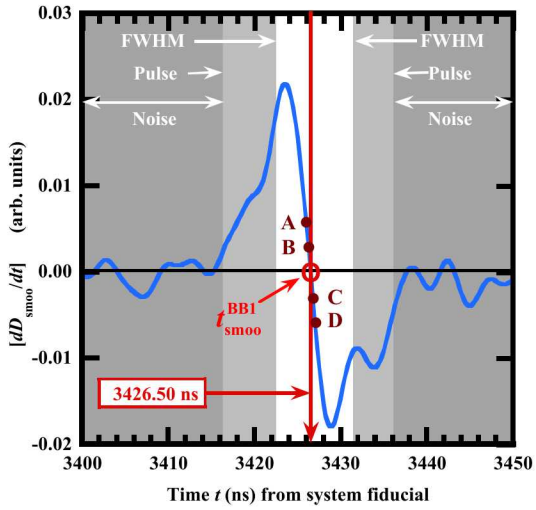

Figure 7. (Color Online) The first derivative of D_{smoo} vs time. The peak time t_{smoo}, taken where dD_{smoo}/dt = 0 is indicated. For reference, derivative values for adjacent time values are shown.: A: 3426.00 ns, B: 3426.25 ns, C: 3426.75 ns, D: 3487.00.

In contrast to treating $D_k(t)$ as a noisy communication signal, one can treat $D_k(t)$ as a pulse-height distribution (Fig. 8) of 0.25-ns-wide bins and apply statistical measures to estimating recorded arrival times.

The first such *statistical* measure (method b, above) is a crude, one-point estimate of the time (t_{mode}) at which the distributional mode occurs (Fig. 8, top). For digitized data, this value may not be unique; and in this case, it is reasonable to average the local times at which the maximum signal occurs. For example, in the noisiest channel (BB1), t_{MAX} = 3426.6 ns with roughly a 1 ns spread.

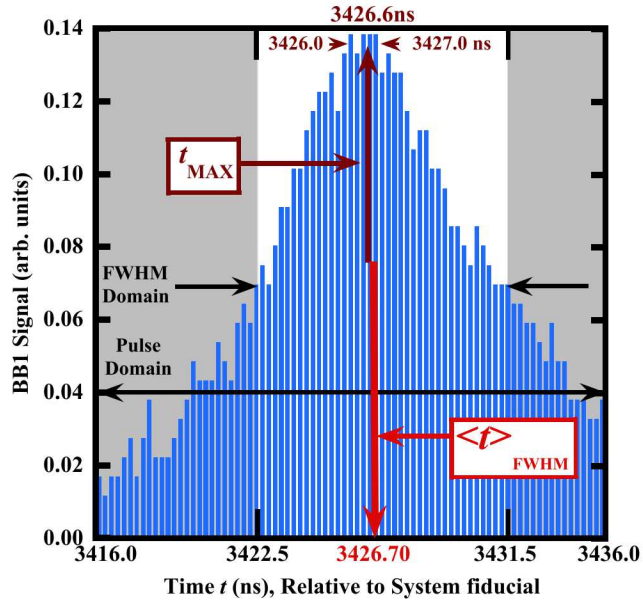

Figure 8. (Color Online) BB1 portrayed as a pulse-height distribution in the FWHM and Pulse domains with corresponding peak measures t_{mode} and $<t>_{FWHM}$.

A second *statistical* measure (method c, above) for defining a pulse-arrival time to the distribution $D_k(t)$ is to estimate a first moment (centroid) $< t >_k \equiv [\Sigma_{j=1}^{N} t_j D(t_j)]/[(\Sigma_{j=1}^{N} D(t_j)]$ over N bins for each nTOF channel k. An advantage of this method is that it averages over more data than the other methods, just noted. However, there is sensitivity to the shape of $D_k(t)$, so that time-domain limits for the averaging process need to be specified. To weaken the influence of baseline noise and distributional skewing at late times, it was decided to restrict the domain for averaging to points within the approximate FWHM of the pulse and the extended 'pulse-width' domain of Figs. 7 and 8. The results were as follows: $< t >_{FWHM}$ = 3426.7 ns (33 pts) and $< t >_{PULSE}$ = 3426.8 ns (80 pts) for the wider domain, an insignificant difference in this example.

In summary, one has the following recorded 'arrival-time' measures for the closest and noisiest nTOF signal (BB1) in shot 2584: (a) S-G smoothing, t_{BB1}^{smoo} = 3426.5 ns; (b) single-point estimate at peak raw signal, t_{mode}^{BB1} = 3426.6 ns; and (c) a centroid within the FWHM, $< t >_{FWHM}^{BB1}$ = 3426.7 ns. The estimates t_{BB1}^{smoo} and t_{mode}^{BB1} appear to have uncertainties of ~1 ns, with uncertainty in $< t >_{FWHM}^{BB1}$ perhaps somewhat smaller.

IV. Results

A. Comparison of recorded Arrival Times for all Channels and methods.

Table 2 compares recorded arrival times for each of the six nTOF detectors in MagLIF shot 2584, analyzed according to the three methods just outlined with sampling times spaced at 0.25 ns.. The times listed are referenced to the system clock in the experiment. The corresponding *times-in-flight* range from ~320 ns to ~1200 ns relative to t_{bang}, given the CODATA value for mean $\bar{u}$ (2.1602 cm/ns) [5] in Eq. (3)].

Distance (cm)	t-smoo (ns)	<t>FWHM (ns)	t-max [raw] (ns)
689.64	3426.50	3426.70	3426.56
785.98	3471.25	3472.10	3471.00
785.98	3472.50	3473.29	3472.50
944.56	3544.20	3544.63	3544.01
1145.85	3638.11	3638.98	3638.11
2510.00	4268.41	4270.40	4268.16

Table 2. Arrival times at each nTOF detector distance in Shot #2584 by the three independent measurement methods in Sect III.D. The centroids $<t>_{FWHM}$ were calculated from the FWHM time regions of the recorded pulses. Entries in each column were then linearly regressed on distance to obtain bang-time and slope estimates.

It is clear from Table 2 that the method-to-method, parametric, arrival-time estimates are fairly tightly grouped with disagreements of □ 1 ns at each distance from the source. For example, arrival time estimates for the dual detector (channels BA2 and BA3) at 786 cm lie in this range. The exception to this trend is the one point $\langle t \rangle_{5A1}$ at 2510 cm, which differs from the other two methods at this distance by 2 ns, perhaps due to noticeable interference in its trace (Fig. 5) at late times. [Whether to keep this point or not in the bang-time estimate was addressed by arbitrarily ignoring this point or otherwise weighting it seeking a better fit. Actually, the fit was not improved and the point was kept.] Overall, however, it seems reasonable to assume that the uncertainties associated with any of these three estimates are not appreciably different and are ~ 1 ns, a conjecture checked in the following linear fitting process.

B. Determination of Bang Time for Shot #2584

Because IRF and PMT-throughput corrections for all the 6 nTOF channels were similar and small (~3—5 ns) compared to expected neutron in-flight times (>350 ns)in, it was decided first to fit Eq. (3) with recorded arrival times (t_{smoo} , t_{mode}, and $\langle t \rangle_{FWHM}$) versus L_k from Tbl. 2 – and later to make the corrections and note changes in the fit parameters.

Figure 10 shows the Least-Squares, equally-weighted, regression of corresponding pairs $\{< t >_k\}_{k=1}^{6}$ upon $\{L_k\}_{k=1}^{6}$, with Eq. (3) used as the fitting function with $\delta t_k \equiv 0$. In this figure, the fit is denoted by the blue solid line; the redlines indicate 95% confidence intervals for single, mean points on the fit line statistics [31,32], *magnified* by a factor of 20×. [Corresponding plots for the other arrival-time estimates $t_{MAX,k}$ and $t_{smoo,k}$ vs L_k are visually indistinguishable on this scale and not shown.] The six *residuals*, $< t >_k$ minus the fit, in Fig. 10 are statistically consistent with a normal distribution of mean 0.0 ns and standard deviation of ~1.14 ns, a result consistent with the uncertainty estimates of arrival times by method above in Table 2. A χ^2/degrees-of-freedom test of these residuals for Fig. 10 has 4 degrees of freedom (6 data residuals minus 2 fit parameters) and a test statistic of 0.7233. According to statistical tables [33], a [2.5%, 97.5%]–test–interval for $\chi_4^2/4$ is 0.121—2.7856, which overlaps the experimental statistic here. (If the uncertainty estimates of arrival times were as low as 0.5 ns or as high as 2 ns, the fit would be considered either 'unlikely' or 'too good to be true', respectively, at 95% confidence.)

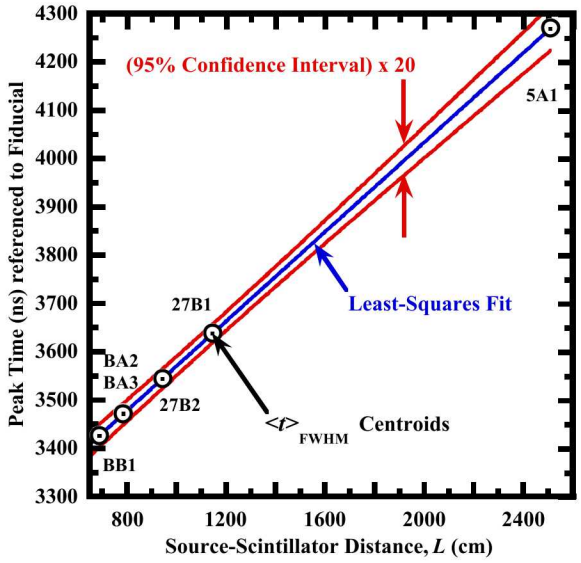

Fig. 9 (Color Online) Least-squares fit to first-moment (centroid) $\langle t \rangle_{FWHM}$ temporal data for the 6 nTOF detectors in shot #2584. Also shown (red lines) are the corresponding 95% confidence intervals (CI) for the mean fit at an arbitrary distance (but not all distances simultaneously). The CI numbers have been multiplied by 20X to be visible on this vertical scale. Data channels (Table 1) are noted.

Shown on the top 3 lines (blue font) of Table 3 are the fit parameters for these recorded arrival times from Tbl. 2 by each method: these include (a) the extrapolated intercept t_{bang} (ns) and its standard error (ns); (b) a 95% confidence interval for t_{bang} (ns); and (c) the fitted slope $(\bar{u})^{-1}$ (ns/cm) and its standard error (ns/cm). To save typographical space, t_{bang} and its confidence interval have been 'encoded': i.e., here 3100 ns has been arbitrarily subtracted from the actual numerical values on the system clock. (Hence, e.g., '8.1' stands for t_{bang} = 3108.1 ns, and '[6.1,10.1]' stands for a confidence interval of [3106.1 ns, 3110.1 ns].) Neither of the standard error columns nor the slope column are encoded and may be read directly.

Method	Intrcpt: SE (ns)		95% CI ns	Slope: SE (ns/cm)	
<t>	8.1:	0.72	[6.1, 10.1]	0.4631:	0.0006
t-max	7.9:	0.69	[6.0, 9.9]	0.4623:	0.0005
t-smoo	8.2:	0.55	[6.6, 9.7]	0.4622:	0.0004
<t>corr	3.0:	0.97	[0.3, 5.6]	0.4646:	0.0007

Table 3. (Color Online) Fit statistics for shot #2584. For each method (first-moment, max peak, and smoothed data), the table lists the estimated mean intercept (bang-time) and its standard error SE (both in ns), the estimated 95% confidence interval (CI) for the intercept (i.e., what time interval would one expect to capture the 'true' intercept for 95% of identical experimental replications), and the slope and its standard error. For typographical convenience, 3100 ns has been arbitrarily subtracted from the fiducially referenced intercepts and CIs in this table. The **<t>corr** entry included the IRF and PMT corrections and would be reportable.

Figure 10 compares the extrapolated t_{bang} of Fig. 9 to show the relationships and 95% confidence intervals in Tbl. 3. The upper part of this figure (blue and red lines) pertains to the same fit of $\langle t \rangle_k$ to L_k as in Fig. 10, except that the 95% confidence intervals are *not* magnified. The bang-time parameter (at L = 0) for this measure is 3108.06 ns relative to the system clock, and the estimated standard error (SE) of the bang time is ~0.7 ns (or alternatively ±2 ns at 95% confidence). Also sketched in Fig. 11 (short, light-blue line) span the corresponding fits and bang times from the raw data using the smoothed and mode methods, both of which have similar uncertainties to the centroid method.

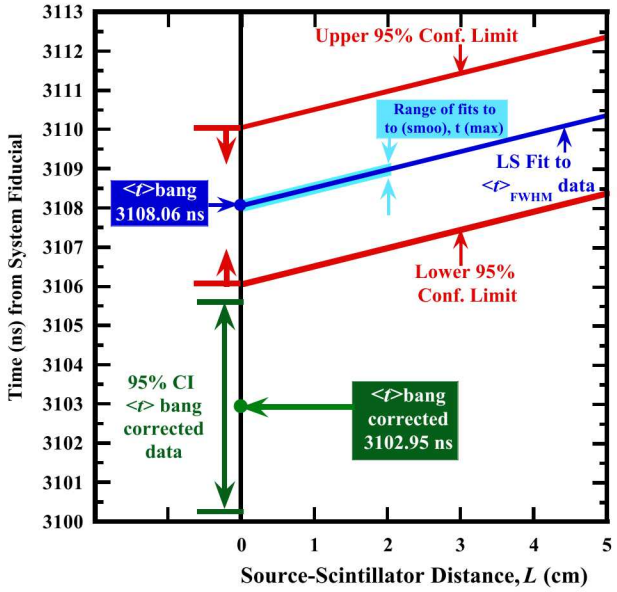

Figure 10 (Color Online). Extrapolated region of arrival time-vs-distance fit curves for shot #2584. The dark blue fit line results from $\langle t \rangle_{FWHM}$ data with 95% confidence uncertainty lines (red); extrapolated fits for the t_{Smoo} and t_{MAX} data are indicated by the short blue line. The green lines below indicate the result after IRF and throughput time corrections.

The lower part of Fig. 11 and the lowest row in Tbl.3 (green font) show the extrapolated results for $\langle t \rangle_{FWHM}$ when the channel signals are first corrected for individual IRF and PMT throughput times and then refit against detector distance ($\delta t_k \neq 0$). One sees in this particular shot that there is an overall early bang-time shift by about 5 ns, while the SE and 95% confidence interval are slightly increased, and the slope parameter $(\bar{u})^{-1}$ [Eq. (3)] is essentially unchanged – an issue rejoined in Sect. V below. The bang-time shift is in accord with estimates already noted (cf. Sect. III.B) [16]. Hence, for shot 2584, one would report [34,35] **<t>corr** = 3102.95 ns for the bang time with an SE = 0.97 ns and 6 measurements [or, equivalently, 3102.95 ns ± 3 ns at 95% confidence and 4 degrees of freedom].

V. Discussion.

The primary purpose of this study was to determine the time of neutron emission (bang time) with estimated uncertainties from the D(d, n)He^3 reaction in a D_2-filled, MagLIF experiment at the Z facility. Time-dependent, current-mode data were provided by an independent,

spatially-separated and calibrated array of nTOF detectors. In this measurement, arrival times for the various data traces were operationally prescribed by three separate methods, and the results could be related to the emitted, uncollided neutron pulse in the midst of interference radiation, noise, and signal distortion. Comparisons showed agreement in bang times of a few nanoseconds after corrections.

We believe that the bang-time estimate and its uncertainty given here present no major difficulties on a on a timescale of a few nanoseconds. To check that assertion there are simpler methods of estimating t_{bang} and $|\delta t_{\mathrm{bang}}|$ *if* one can assume that the neutron distribution is due to DD neutrons (i.e., $\overline{u}$ = 2.016018587 cm/ns [5]). Firstly, if Eq.(3) is summed over the $N = 6$ nTOF arrival times t_k (by whatever peak criterion or correction) and distances L_k, one finds a simple average estimate as $\langle t_{\mathrm{bang}} \rangle \cong < t_k >_N - (1/\overline{u}) < L_k >_N$, which here yields 3105.35 ns compared to 3102.95 ns with the detailed, corrected data in Fig. 10, and Tbl. 3. Secondly, $|\delta t_{\mathrm{bang}}|$ can be estimated if one is willing to provide uncertainties (δt and δL) for peak times and distance. Experimentally, It is assume experimentally $\delta t \approx$ 1 ns and $\delta L \approx$ 1 cm as upper bounds. Then, by error propagation in Eq. (3) one has $(\delta t_{\mathrm{bang}})^2 \approx (\delta t_k)^2 + (\delta L_k)^2 / \overline{u}^2$, which gives $\delta t_{\mathrm{bang}} \approx \pm 1$ ns – again with the assumption that $\overline{u}$ is known. (This estimate, of course, no use of N channels, which would reduce this estimate by $\sim\sqrt{N}$. Both these crude estimates are consistent with the more detailed estimates above.

If the primary goal of this nTOF diagnostic was to determine bang times, a secondary goal was to check the provenance of the neutrons pulses under test – in particular, to assess evidence that might invalidate the assumption that these neutrons arise from the D(d,n)He^3 reaction. Specifically, according to the Brysk model, one should find (a) isotropic neutron emission and (b) an approximate Gaussian, speed-distribution with average mean speed $\overline{u}$ = 2.16 cm/ns and a mean neutron kinetic energy $\overline{E}$ = 2.45 MeV [5].

The spectral shape of the emitted neutron distribution here is beyond this study since only the first moment was addressed. But, one can address the isotropy issue by examining the fits to this moment as a function of distance from the source. Specifically, the strongly linear least-squared fits observed in Figs.10 and 11 are actually consistent with isotropy at least to within a nanosecond timescale. If, for example, the neutron distribution varied significantly with emission angle, one would expect noticeable non-linear behavior which is not observed.

Putting the distributional shape of neutron emission aside, however, one can estimate the mean speed $\overline{u}$ of the neutron pulses from the nTOF data in shot #2584. By the linear fitting model Eq.(3) the slopes of the curves in Figs.9 and 10 are estimates of ($1/\overline{u}$), so that one finds from the *corrected* data (Tbl. 3, line 4, green font) a slope of 0.464617 ns/cm with standard error of 0.000743 ns/cm and $\overline{u}$ = 2.1523 ± 0.0096 cm/ns (@ 95% confidence, 4 degrees of freedom). This may be compared to the published value of 2.1601 8587 cm/ns [5] for D-D fusion neutrons. The relative precision of this estimate can be crudely approximated from Eq.(3) similar to above: let $\overline{u} \equiv L_k/(t_k - t_{\mathrm{bang}})$, then one has $(\delta\overline{u})^2 (t_k - t_{\mathrm{bang}})^2 \approx (\delta L_k)^2 + \overline{u}^2[(\delta t_k)^2 + (\delta t_{\mathrm{bang}})^2]$ by error propagation. For, say, the detector at L_{27B2} = 945 cm (Tbl. 1) and the arbitrary guesses $\delta L_k \approx 1$ cm and $\delta t_k = \delta t_{\mathrm{bang}} \approx 1$ ns, one has $(\delta\overline{u}/\overline{u}) \approx 0.0034$ or $\delta\overline{u} \approx 0.0074$ cm/ns which compares well with the slope estimates. [Here we have used the published 2.1602 cm/ns for $\overline{u}$ and not the full ensemble of data channels.]

With the experimental value $\overline{u}$ = 2.1523 ± 0.0096 cm/ns, one can estimate the relativistic mean kinetic energy $\overline{E}$ of the detected neutron distribution from $\overline{E} = m_0c^2[(1 - \overline{u}^2/c^2)^{-1/2} - 1]$. This calculation gives 2.4308 MeV ± 0.0223 Mev – alternatively, [2.408014, 2.452611] MeV CI with 4 degrees of freedom – and overlaps the published value of 2.4486857 MeV [5]. (Here, m_0c^2 was taken as 939.565379 MeV and c as 29.9792458 cm/ns [5].)

Therefore, the fact that both $\overline{u}$ and $\overline{E}$ in shot #2584 were consistent with published values to within 1% is clear evidence the detected neutrons were largely produced by D-D interactions. Finer details in their production were beyond the experiment.

Future work with this nTOF apparatus of the type here will depend on the specific goals of this measurement. For example, if the only goal is *routinely* to define bang-time and to leave other diagnostics to probe the neutron spectral shape, then a simpler version with (say) two separated dual-scintillator nTOF probes may be acceptable: such an arrangement would free up two lines of sight, provide backup data should one channel of each dual probe fail, and provide at least independent channels if all signals are obtained. On the other hand, if the goal is to extend this method to the detailed shape of the neutron distribution, more attention must be paid to understanding and ameliorating the effects of background interferences and detector responses.

References

1. I. Estermann; O. C. Simpson, O. Stern, *Phys. Rev.* **71(4)**, 238 (1947)

2. L. C. L. Yuan, S. J. Lindenbaum, "Determination of Velocity: Time-of-Flight Method," Sect. 2.2.1.3.1, *Methods of Experimental Physics A*, L. C. L. Yuan and C-S Wu, eds. Nuclear Physics, part A (Academic Press, New York, 1961) p.438 ff.

3. R. Rosen, D. W. Miller, "Differential Interaction Cross Sections", Section 2.7.5, in *Methods of Experimental Physics B*, L. C. L. Yuan and C-S Wu, eds. Nuclear Physics, part A (Academic Press, New York, 1963) p.456 ff.

4 H. Brysk *Plasma Phys*, **15** 611 (1973).

5 D. H. Munro, *Nuclear Fusion*, **56(3)** 036001 (2016).

6. R. A. Lerche, V. Yu. Glebov, J. J. M. M. Moran, et al., "National Ignition Facility neutron time-of-flight measurements," *Rev. Sci. Instrum*. 81, 10D319 (2010)

7. R. Hatarik, D.B. Sayre, J. A. Caggiano, T. Phillips, M. J. Eckart, E. J. Bond, C. Cerjan, G. P. Grim, E. P. Hartouni, J. P. Knauer, J. M. Mcnaney, and D. H. Munro. *J. Appl. Phys.,* **118**, 184502 (2015).

8. T. J. Murphy, R. E. Chrien, and K. A. Klare, *Rev. Sci. Intrum.* **68**(1), 610 (1997).

9. T. J. Murphy and R. A. Lerche, C. Bennett, and G. Howe, *Rev. Sci., Instrum*., **66**, 930 (1995).

10. T. J. Murphy, J. L Jimerson, R.R. Bergren, J. R. Faulkner, J. A Oertel, P. J. Walsh. *Rev. Sci. Instrum.,* **72**, 850 (2001).

11. S. A. Slutz, et al., Phys. Plasmas 17, 056303 (2010)

12. M. Gomez, et al., *Phys. Rev. Lett*. **113** (2014)

13. S. Hanson, "Progress in Magnetized Liner Inertial Fusion (MagLIF), European Physical Society Conference on Plasma Physics, (June 22-26 2015).

14. R. B Spielman, C. Deeney, G. A. Chandler, et al., *Phys. Plasmas* **5**, 2105.

15. W. A. Stygar, H. C. Ives, D. L. Fehl, et al., *Phys. Rev. E*, **69**, 046403 (2004).

16. M. A Bonura, C. L. Ruiz, D. L. Fehl, G. W. Cooper, G. Chandler, K. D. Hahn, A. J. Nelson, J. D. Styron, and J. A. Torres. *Rev. Sci. Instrum*., **85**, 11D633 (2014).

17. C. L. Ruiz, et al., *Phys. Rev. Lett.*, **94**(1), 015001 (2004)]

18. W. H. Press, S. A. Teukolsky, W. T. Vetterling, and B. P. Flannery, *Numerical Recipes in FORTRAN: The Art of Scientific Computing*, 2nd Ed. (Cambridge University Press, NY. 1992) Sect. 14.8, p .644 ff.

19. Wikipedia, Savitzky-Golay filter https://en.wikipedia.org/wiki/Savitzky_Golay_filter.

20. C. Stoeckl, M. Cruz, V. Yu. Glebov., J. Knauer, *Rev. Sci. Instrum.*, **81** 10D302 (2010).

21. ***PeakFit™ User's v4 Guide Manual*,** For Windows (SeaSolve Software, Inc., 235 Walnut St., Suite 7, Framingham, MA 01702. USA, ©2003, ISBN 81-88341-07-X), section 7 (esp. p. 7-68ff).

22 K. Lan, and J. W. Jorgenson, *J. Chromatogr. A*, **915,** 1 (2001).

23 A useful summary of results for this function is given in Wikipedia, "Exponentially Modified Gaussian Function," https://en.wikipedia.org/wiki/Exponentially_modified_Gaussian_distribution. Derivations of the EMG are given by C. Wheldon, "Convolution of a Gaussian with an exponential (and its application in programs halflife.c/nanofit.f), posted on line (2014)l; S. Haney, "Practical Application and Properties of the Exponentially Modified Gaussian (EMG) Function, and (PhD Thesis, Drexel University) 23 March 2011. The function 'erfcx(t)' is tabulated in H. S. Carslaw and J. C. Jaeger, *Conduction of Heat in Solids*, 2nd Ed., (Oxford University Press, London, 1959), Table I, "The error function and its derivatives and integrals," the leftmost columns, p. 485. Some history and applications are given in E. Grushka, *Anal. Chem.*, **42**, 21 (1970); P. A. Gorry, *Anal. Chem*, **62** 570 (1990); Yu. Kalambet, Yu. Kozmin, K. Mikhailova, I. Nagaev, and P. Tikhonov. *J. Chemometrics*, **25**, 352 (2011). It should be noted that models for impulse (instrumental) responses represent an active research field for many applications, and the reader should be warned that the mathematical notation as well as the normalizations (e.g. peak or integral) vary: see J. Li, *J. Chromatogrr. Sci.*, **33** 568 (1995). Lastly, See E. W. Ng and M. Geller, "A Table of Integrals of the Error Functions," *J. Res. NBS – Mathematical Sciences*, **73B**(1) 1 (1968).

24 . H. H. Barrett and W. Swindell, *Radiological Imaging: The Theory of Image Formation, Detection, and Processing*, Vol. 1 (Academic Press, New York, 1981)

25 M. Bertero, "Linear Inverse and Ill-Posed Problems," in *Advances in Electronics and Electron Physics*, vol. 75 edited by P. W. Hawkes (Academic Press, Harcourt Brace Jovanovich, Boston, 1989), pp 2-120.

26 I. J. D. Craig and J. C. Brown, *Inverse Problems in Astronomy: a guide to inversion strategies for remotely sensed data*, (Adam Hilger Ltd, Boston ,1986), Sect. 4.3.

27 G. M. Wing, *A Primer on Integral Equations of the First Kind: The Problem of Deconvolution and Unfolding* (Society for Industrial and Applied Mathematics, SIAM, Philadelphia,1991), p.71.

28. D. L. Fehl, G. A. Chandler, W. A. Stygar, R. E. Olson, C. L. Ruiz, J. J. Hohlfelder, L. P. Mix, F. Biggs, M. Berninger, P. O. Frederickson, and R. Frederickson, *Phys. Rev. Special Topics – Accelerators and Beams* **13**, 120402 (2010)

29 Bromiley, P. A., "Products and Convolutions of Gaussian Probability Density Functions," Internal Report, TINA Memo No. 2003-003 (Imaging Sciences Research Group, Institute of Population Health, School of Medicine, University of Manchester, Stopford Building, Oxford Road, Manchester, M13 9PT, UK) 14 Aug. 2014. paul.bromiley@manchester.ac.uk.

30 R. N. Bracewell, *The Fourier Transform and Its Applications*, 2nd Edition (McGraw-Hill Book Co., New York, 1978) pp. 108-119.

31 M. G. Natrella, *Experimental Statistics* (Dover Publications, Inc., Mineola, NY, 2005, a republication of National Bureau of Standards Handbook 91, issued in 1963), chapter 5

32 J. Neter, M. H. Kutner, C. J. Nachtsheim, and W. Wasserman, *Applied Linear Regression Models*, 3rd edition, (R. D. Erwin, Inc., Chicago, 1996) p.44 ff.]

33 *CRC standard probability and statistics tables and formulae*, W. H. Beyer (editor), (CRC Press, inc., Boca Raton, FL, 1991), p. 207 ff.

34 B. N. Taylor and C. E. Kuyatt, "Guidelines for Evaluating and Expressing the Uncertainty of NIST Measurement Results," ***NIST Technical Note* 1297,** (National Institute of Standards and Technology, Gaithersburg, MD 20899 (1994).],

35 T. M. Adams, "G104 – A2LA Guide for Estimation of Measurement Uncertainty In Testing,"(2002)]